Steel and Composite Structures, *Vol. 22, No. 2 (2016) 301-321*
DOI: http://dx.doi.org/10.12989/scs.2016.22.2.301

Buckling analysis of laminated composite cylindrical shell subjected to lateral displacement-dependent pressure using semi-analytical finite strip method

Majid Khayat [1a], Davood Poorveis [*1] and Shapour Moradi [2b]

[1] *Department of Civil Engineering, Shahid Chamran University of Ahvaz, Iran*
[2] *Department of Mechanical Engineering, Shahid Chamran University of Ahvaz, Iran*

(*Received March 28, 2016, Revised September 30, 2016, Accepted October 05, 2016*)

Abstract. The objective of this paper is to investigate buckling behavior of composite laminated cylinders by using semi-analytical finite strip method. The shell is subjected to deformation-dependent loads which remain normal to the shell middle surface throughout the deformation process. The load stiffness matrix, which is responsible for variation of load direction, is also throughout the deformation process. The shell is divided into several closed strips with alignment of their nodal lines in the circumferential direction. The governing equations are derived based on the first-order shear deformation theory with Sanders-type of kinematic nonlinearity. Displacements and rotations of the shell middle surface are approximated by combining polynomial functions in the meridional direction and truncated Fourier series along with an appropriate number of harmonic terms in the circumferential direction. The load stiffness matrix, which is responsible for variation of load direction, is also derived for each strip and after assembling, global load stiffness matrix of the shell is formed. The numerical illustrations concern the pressure stiffness effect on buckling pressure under various conditions. The results indicate that considering pressure stiffness causes buckling pressure reduction which in turn depends on various parameters such as geometry and lay-ups of the shell.

Keywords: deformation-dependent loads; finite strip method; buckling behavior; laminated composite; cylindrical shells

1. Introduction

Structures are subjected to wide variety of forces, which can be classified into two categories, including: conservative and non-conservative forces. Stability of structures, under deformation-dependent loads, depends on the loading type, body attached or space attached, load distribution; moreover, shell boundary conditions, can be categorized under conservative or non-conservative title. In the case of conservative loads, static criterion (divergence) can be used to produce symmetric global stiffness matrix. Non-conservative loads can divide the system into purely and hybrid non-conservative systems. The first group only fails by flutter and so the kinetic criterion, which connects computing buckling loads to vibration equation of structure, governs. In the hybrid

*Corresponding author, Ph.D., E-mail: dpoorveis@scu.ac.ir
[a] M.Sc. Student, E-mail: khayatmajid@yahoo.com
[b] Ph.D., E-mail: moradis@scu.ac.ir

http://www.techno-press.org/?journal=scs&subpage=6 ISSN: 1229-9367 (Print), 1598-6233 (Online)

case, both criteria, static or kinetic, can dominate the problem (Datta and Biswas 2011, Argyris and Symeonidis 1981). Displacement-dependent loads can be caused by contact of structures with liquid or gaseous media resulting in pressure forces acting normal to the contact surfaces and forces acting tangential to the surfaces.

The buckling phenomenon consists of a sudden change of equilibrium configuration at a certain critical load. Buckling has a crucial role in the behavior of thin-walled structures such as plates and shells. Since the load carrying capacity of thin-walled members is frequently dependent on buckling phenomena, the ability to calculate the associated elastic critical loads is of great importance. If a linear initial equilibrium path is also assumed, linearized stability analysis reduces the determination of the critical load to a linear eigenvalue problem (Euler's method) (Nali *et al*. 2011).

Anastasiadis and Simitses (1993) compared the classical theories, first order and higher order shear deformations shell theories, to calculate buckling load of composite cylindrical shells under axial and lateral pressures; furthermore, they checked the effects of different parameters on buckling load calculated by different theories. In Shen's (1988) study, post-buckling analysis was presented for a shear deformable cross-ply laminated cylindrical shell of finite length subjected to combined loading of external pressure and axial compression. The governing equations in this paper are based on Reddy's higher order shear deformation shell theory. Matsunaga (2007) analyzed natural frequencies and buckling stresses of cross-ply laminated composite circular cylindrical shells by considering the effects of higher-order deformations. Therefore, the investigator used power series expansion to describe displacement components. Ovesy and Fazilati (2009) presented finite strip method to analyze linear and non-linear buckling of composite plate and cylindrical shell. They used Sanders's theory for linear and Donnell's theory for non-linear analyses. In Li and Lin's (2010) study, a post-buckling analysis was presented for a shear deformable anisotropic laminated cylindrical shell with stiffeners; moreover, the researchers used higher order shear deformation shell theory with von Karman-Donnell-type of kinematic nonlinearity and stiffener modeling by considering the smeared method. Zielnica (2012) studied the buckling loads and stability paths of a sandwich conical shell with unsymmetrical faces under combined loads based on the assumptions of moderately large deflections. Tornabene *et al*. (2014) evaluated the free vibration of free-form doubly-curved shells made of functionally graded materials using higher-order equivalent single layer theories. Tornabene *et al*. (2015) estimated the behavior of doubly-curved composite deep shells with variable radii of curvature under concentrated loads by a new approach. The paper showed convergence, stability and accuracy of the presented approach when applied to beams, plates and doubly-curved thin and thick shells. Jung *et al*. (2016) presented post-buckling behavior of laminated composite plates and shells, subjected to various shear loadings, using a modified finite element method.

Bolotin (1963) was one of the pioneering researchers who studied the effects of load behavior on structures stability. He categorized loads in to dead and follower types. In dead loads, both magnitude and direction of load remain constant during loading process. However, in the case of follower loads, the magnitude is constant but the direction changes. He also extracted conditions for uniformly distributed load over the external surface of a body in which remains normal to the deformed surface in order to be conservative. In addition, it has been concluded that if the forces are non-conservative, the form, which the loss of stability is assumed, requires special investigation in each problem. Both instability types are possible in this case. In many problems, based on the relations which exist between the parameters, the minimum critical loads correspond to either the static or the oscillatory (flutter) stability loss. Another research which studied conservativeness of a normal pressure field acting on a shell, has been accomplished by Cohen (1966). He not only confirmed the Bolotin's research for flat plates but also generalized the results to a non-uniform continuous normal pressure field acting on an arbitrary shell. Afterwards, he modified the potential energy of loading to incorporate shells of arbitrary curvature. Romano (1971) extracted through the potential operator theory to present the correct proof of conservativeness condition. The analysis was performed in the large (finite deformation) obtaining a general condition for conservativeness of pressure loading. Sheinman and Tene (1974) emphasized on the functional potential energy derived by Cohen (1966); however, they suggested another expression for the normal pressure potential energy. Hibbitt (1979) extracted the contribution of follower forces to the tangent stiffness matrix which can be called load stiffness matrix. Generally, this matrix is un-symmetric but in special cases, it can appear as a symmetrical matrix. Due to non-uniform pressure, the investigator also demonstrated that the magnitude of non-symmetric matrix can be decreased by refining meshes while other aspects of non-symmetry are not dependent on element sizes. Schweizerhof and Ramm (1984) studied displacement-dependent pressure loads in nonlinear finite element analysis. They evaluated specific conditions when a pressure load is conservative and vice versa. The important part of their work was to propose a load classification into body attached and space attached loads. In the body attached case, load stiffness matrix was divided into four parts so that three parts including two parts containing integrals along boundaries and the other related to variation of loading magnitude in the domain were skew-symmetric matrices. In the case of uniform pressure, the potential conditions were similar to those obtained by other researches. Altman *et al*. (1988, 1990) studied vibration and stability of cylindrical shell panels under follower forces. The obtained solution (Eigen curves) was used in conjunction with the dynamic criterion of stability to find the critical values of the frequency and loading parameters. Iwata *et al*. (1991) derived a symmetric load-stiffness matrix for buckling analysis of shell structures under uniform pressure loads. It should be noted that in finite element method, in order to execute large deformation analysis and to calculate the buckling load, it is necessary to introduce a load-stiffness or load correction matrix as well as the conventional linear and geometrically non-linear (initial stress) stiffness matrices. Therefore, they used the results obtained by Schweizerhof and Ramm (1984). Park and Kim (2002) tried to reasonably simulate behavior of rockets or missile. They analyzed dynamic stability of completely free cylindrical shells under axial follower force for a specific situation in which the edge of shell is movable but not freely deformable. By executing geometric nonlinear analysis, Lazzari *et al*. (2003) carried out the study of large lightweight roof structures under the dynamic effects of the turbulent actions caused by wind. The wind loads were considered as deformation-dependent forces. Wang (2003) studied a beam structure subjected to a static follower force. The beam was fixed in the transverse direction and constrained by a rotational spring at one end, and by a translational spring and a rotational spring at the other end. Poorveis and Kabir (2006) estimated buckling of discretely stringer-stiffened composite cylindrical shells under combined axial compression and external pressure in the form of live (follower) pressure. Cagdas and Adali (2011) investigated buckling of cross-ply cylinders under hydrostatic pressure by considering pressure stiffness (PS) and regarding semi-analytical finite element method. Khayat *et al*. (2016) investigated the effect of pressure stiffness on buckling of thick deep shells.

The present paper is concerned with study on the linear buckling analysis of laminated composite cylindrical shells by semi-analytical finite strip method. First, the fundamental equations for the buckling analysis of shell segments based on shell theory and adjacent equilibrium criterion have been derived. Then, the exact expression for calculating the pressure stiffness matrix due to the follower pressure for cylindrical shell has been developed. Finally, the effects of various parameters such as lengths to radius ratio and thickness of shell, shell boundary conditions and shell lay-up on the buckling pressure of the cylindrical shells have been discussed.

2. Methodology

2.1 Shell geometry and coordinates system

The position of a shell point is given by: (θ) as the circumferential coordinate, (s) as the meridional coordinate and (z) as the coordinate in the normal to the middle surface that are shown in Fig. 1.

It should be noted that, owing to weakness of composite material in shear rigidity, in this article, the first-order shear deformation theory has been utilized. Therefore, the displacement field corresponding to the first order shear deformation theory is given as

$$\begin{aligned} \bar{u}(s,\theta,z) &= u(s,\theta) + z\beta_s \\ \bar{v}(s,\theta,z) &= v(s,\theta) + z\beta_\theta \\ w(s,\theta,z) &= w(s,\theta) \end{aligned} \tag{1}$$

where: u, v and w are displacements in the middle surface of the laminate and β_s, β_θ are the rotations of the normal vector of the middle plane around the θ and s axes, respectively.

2.2 Semi-analytical finite strip method

The shell is divided into several closed strips with alignment of their nodal lines in the circumferential direction. Displacements and rotations in the shell middle surface are approximated by combining polynomial functions in the meridional direction and truncated Fourier series with an appropriate number of harmonic terms in the circumferential direction. The circumferential variation of the displacements u, v and w and rotations β_s and β_θ can be described

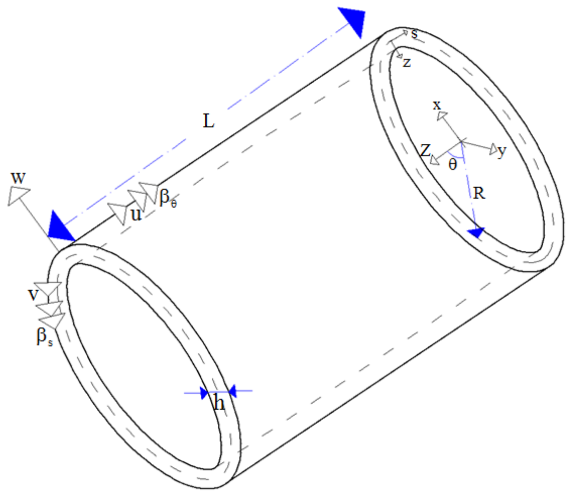

Fig. 1 Coordinates system

by a suitable Fourier series expansion which in general consists of both symmetric and anti-symmetric terms

$$
\begin{aligned}
u(s,\theta) &= u^{c_o}(s) + \sum_{k=1}^{NH}\left[u^{c_n}(s)\cos(kn_{cr}\theta) + u^{s_n}(s)\sin(kn_{cr}\theta)\right] \\
v(s,\theta) &= v^{c_o}(s) + \sum_{k=1}^{NH}\left[v^{c_n}(s)\cos(kn_{cr}\theta) + v^{s_n}(s)\sin(kn_{cr}\theta)\right] \\
w(s,\theta) &= w^{c_o}(s) + \sum_{k=1}^{NH}\left[w^{c_n}(s)\cos(kn_{cr}\theta) + w^{s_n}(s)\sin(kn_{cr}\theta)\right] \\
\beta_s(s,\theta) &= \beta_s^{c_o}(s) + \sum_{k=1}^{NH}\left[\beta_s^{c_n}(s)\cos(kn_{cr}\theta) + \beta_s^{s_n}(s)\sin(kn_{cr}\theta)\right] \\
\beta_\theta(s,\theta) &= \beta_\theta^{c_o}(s) + \sum_{k=1}^{NH}\left[\beta_\theta^{c_n}(s)\cos(kn_{cr}\theta) + \beta_\theta^{s_n}(s)\sin(kn_{cr}\theta)\right]
\end{aligned} \tag{2}
$$

where θ and s stand for circumferential and meridional coordinates, respectively. k represents a coefficient and NH is the number of terms in the truncated series. Superscript c_o exhibits contribution of axisymmetric part of displacements and rotations while c_n and s_n emphasize on presence of cosine and sine functions in the shell deformations and n_{cr} is the circumferential wave number. The displacement and rotation expansions apply for both pre-buckling state and buckling modes. The number of harmonics used in the analyses depends on the subjected loads as well as material anisotropy. In the case of uniform axisymmetric, axial or lateral pressure and material isotropy, only axisymmetric terms are active in the pre-buckling state. On the other hand, for buckling mode, only one wave number which leads to the minimum buckling loads is involved in the analysis. Generally, when a shell made by coupling material stiffness is subjected to partial deformation dependent loadings, full expansions are required for both pre-buckling and buckling states.

2.3 Strain-displacement relations

The generalized strain vector can be written as follows

$$
\varepsilon^T = \{\varepsilon_{ss} \quad \varepsilon_{\theta\theta} \quad \gamma_{s\theta} \quad \kappa_{ss} \quad \kappa_{\theta\theta} \quad \kappa_{s\theta} \quad \gamma_{sz} \quad \gamma_{\theta z}\} \tag{3}
$$

The strain-displacement relations at an arbitrary point of the shell thickness can be expressed as follows

$$
\bar{\varepsilon}_{ss} = \varepsilon_{ss} + zk_{ss} \qquad \bar{\varepsilon}_{\theta\theta} = \varepsilon_{\theta\theta} + zk_{\theta\theta} \qquad \bar{\gamma}_{s\theta} = \gamma_{s\theta} + zk_{s\theta} \tag{4}
$$

where linear strain-displacement relations are (Teng and Hong 1998)

$$
\varepsilon_{ss} = \frac{\partial u}{\partial s} \qquad \varepsilon_{\theta\theta} = \frac{1}{R}\frac{\partial v}{\partial \theta} + \frac{w}{R} \qquad \gamma_{s\theta} = \frac{\partial v}{\partial s} + \frac{1}{R}\frac{\partial u}{\partial \theta} \tag{5}
$$

moreover, the transverse shear strains can be calculated as follows

$$
\gamma_{sz} = \beta_s + \frac{\partial w}{\partial s} \qquad \gamma_{\theta z} = \beta_\theta + \frac{1}{R}\frac{\partial w}{\partial \theta} - \frac{v}{R} \tag{6}
$$

where the bending curvatures, k_{ss}, $k_{\theta\theta}$ and torsional curvature $k_{s\theta}$ are expressed as

$$\mathrm{k}_{ss}=\frac{\partial\beta_s}{\partial s}\qquad \mathrm{k}_{\theta\theta}=\frac{1}{R}\frac{\partial\beta_\theta}{\partial\theta}\qquad \mathrm{k}_{s\theta}=\frac{\partial\beta_\theta}{\partial s}-\frac{1}{R}\frac{\partial\beta_s}{\partial\theta}+\frac{1}{R}\frac{\partial v}{\partial s} \tag{7}$$

The nonlinear strain-displacement relations can be calculated based on Sanders's non-linear shell theory as below

$$\begin{aligned}
\varepsilon_{ss}&=\frac{1}{2}\left(\frac{\partial w}{\partial s}\right)^2+\frac{1}{2}\left(\frac{\partial u}{\partial s}\right)^2+\frac{1}{2}\left(\frac{\partial v}{\partial s}\right)^2\\
\varepsilon_{\theta\theta}&=\frac{1}{2R^2}\left(\frac{\partial w}{\partial\theta}-v\right)^2+\frac{1}{2R^2}\left(\frac{\partial v}{\partial\theta}+w\right)^2+\frac{1}{2R^2}\left(\frac{\partial u}{\partial\theta}\right)^2\\
\varepsilon_{s\theta}&=\frac{1}{R}\frac{\partial w}{\partial s}\left(\frac{\partial w}{\partial\theta}-v\right)+\frac{1}{R}\frac{\partial v}{\partial s}\left(\frac{\partial v}{\partial\theta}+w\right)+\frac{1}{R}\frac{\partial u}{\partial s}\frac{\partial u}{\partial\theta}
\end{aligned} \tag{8}$$

2.4 Constitutive equations

The vector of stress resultants is defined as Eq. (9)

$$\sigma=\left\{\mathrm{N}_{ss}\ \ \mathrm{N}_{\theta\theta}\ \ \mathrm{N}_{s\theta}\ \ \mathrm{M}_{ss}\ \ \mathrm{M}_{\theta\theta}\ \ \mathrm{M}_{s\theta}\ \ \mathrm{Q}_{sz}\ \ \mathrm{Q}_{\theta z}\right\}^{T} \tag{9}$$

N_{ss}, $N_{\theta\theta}$ and $N_{s\theta}$ a are designated as the in-plane meridional and circumferential normal stress resultants and shear stress resultant respectively. M_{ss}, $M_{\theta\theta}$ and $M_{s\theta}$ are the analogous couples, while Q_{sz} and $Q_{\theta z}$ represent the transverse shear stress resultants. The constitutive equations relate internal stress resultants and internal couples with generalized strain components on the middle surface

$$\begin{Bmatrix}\mathrm{N}_{ss}\\ \mathrm{N}_{\theta\theta}\\ \mathrm{N}_{s\theta}\\ \mathrm{M}_{ss}\\ \mathrm{M}_{\theta\theta}\\ \mathrm{M}_{s\theta}\\ \mathrm{Q}_{sz}\\ \mathrm{Q}_{\theta z}\end{Bmatrix}=\int_{-h/2}^{h/2}\begin{Bmatrix}\sigma_{ss}\\ \sigma_{\theta\theta}\\ \tau_{\theta s}\\ z\sigma_{ss}\\ z\sigma_{\theta\theta}\\ z\tau_{\theta s}\\ \tau_{sz}\\ \tau_{\theta z}\end{Bmatrix}dz=\begin{bmatrix}A_{11}&A_{12}&A_{16}&B_{11}&B_{12}&B_{16}&0&0\\ A_{12}&A_{22}&A_{26}&B_{12}&B_{22}&B_{26}&0&0\\ A_{16}&A_{26}&A_{66}&B_{16}&B_{26}&B_{66}&0&0\\ B_{11}&B_{12}&B_{16}&D_{11}&D_{12}&D_{16}&0&0\\ B_{12}&B_{22}&B_{26}&D_{12}&D_{22}&D_{26}&0&0\\ B_{16}&B_{26}&B_{66}&D_{16}&D_{26}&D_{66}&0&0\\ 0&0&0&0&0&0&A_{44}&A_{45}\\ 0&0&0&0&0&0&A_{45}&A_{55}\end{bmatrix}\begin{Bmatrix}\varepsilon_{ss}\\ \varepsilon_{\theta\theta}\\ \gamma_{s\theta}\\ k_{ss}\\ k_{\theta\theta}\\ k_{s\theta}\\ \gamma_{sz}\\ \gamma_{\theta z}\end{Bmatrix} \tag{10}$$

A_{ij} stands for extensional stiffness, B_{ij} is called as bending-extensional coupling stiffness and D_{ij} represent bending stiffness which are defined as follows

$$\begin{aligned}
&\left(A_{ij},B_{ij},D_{ij}\right)=\int_h\left(1,z,z^2\right)\bar{Q}_{ij}dz\qquad i\,,j{=}1,2,6\\
&A_{ij}=K\int_h\bar{Q}_{ij}dz\qquad i\,,j{=}4,5
\end{aligned} \tag{11}$$

In addition, c denote the transformed reduced stiffness coefficients. The material properties are assumed to be identical in all layers and the fiber orientations may be different among the layers. *K* in the above equations is shear correction coefficient, typically taken at 5/6.

2.5 Linear elastic and geometric stiffness matrices

The linear part of internal virtual work of shell of revolution is as follows

$$\delta W_{int}^{L} = \int_{\varphi}\int_{\theta}\int_{z} \left(\sigma_{ss}\delta\varepsilon_{ss}^{l} + \sigma_{\theta\theta}\delta\varepsilon_{\theta\theta}^{l} + \tau_{s\theta}\delta\gamma_{s\theta}^{l} + \tau_{sz}\delta\gamma_{sz}^{l} + \tau_{\theta z}\delta\gamma_{\theta z}^{l}\right) dz d\theta d\varphi \tag{12}$$

Integration of Eq. (12) in the thickness direction and by using Eq. (10), the internal virtual work can be written

$$\delta W_{int}^{L} = \int_{0}^{l_o}\int_{0}^{2\pi} (N_{ss}\delta\varepsilon_{ss}^{L} + N_{\theta\theta}\delta\varepsilon_{\theta\theta}^{L} + N_{s\theta}\delta\gamma_{s\theta}^{L} + M_{ss}\delta k_{ss}^{L} + M_{\theta\theta}\delta k_{\theta\theta}^{L} + M_{s\theta}\delta k_{s\theta}^{L} + Q_{ss}\delta\gamma_{ss}^{L} + Q_{\theta\theta}\delta\gamma_{\theta\theta}^{L}) R d\theta ds \tag{13}$$

In which lo is the length of shell meridian. Discretization of δW_{int}^{L} by using Eqs. (2), (5)-(7) and (10) gives

$$\delta W_{int}^{L} = \sum_{j=1}^{nstrip} (\delta\Delta_j)^T K_{ej} \Delta_j \tag{14}$$

In this equation, Δ_j contains all unknown coefficients of displacements and rotations of jth strip and $\delta\Delta_j$ represents its virtual counterpart, also K_{ej} is the linear stiffness matrix of *j*th strip. To form geometric or initial stress stiffness matrix, it is required to carry out a pre-buckling static analysis to obtain in-plane forces, N_{ss}^{o}, $N_{\theta\theta}^{o}$, and $N_{s\theta}^{o}$ for each strip in the gauss points. Then the internal virtual works of these real membrane forces in non-linear virtual strains are in the form

$$\delta W_{int}^{NL} = \int_{s}\int_{\theta} \left(N_{ss}^{o}\delta\varepsilon_{ss}^{NL} + N_{\theta\theta}^{o}\delta\varepsilon_{\theta\theta}^{NL} + N_{s\theta}^{o}\delta\gamma_{s\theta}^{NL}\right) R d\theta ds \tag{15}$$

Discretization of δW_{int}^{nL} by using Eqs. (2) and (15) gives

$$\delta W_{int}^{NL} = \sum_{j=1}^{nstrip} (\delta\Delta_j)^T K_{Gj} \Delta_j \tag{16}$$

In which K_{Gj} represents the geometric stiffness matrix of jth strip. Assembling of K_{ej} and K_{Gj} of all strips result in global linear elastic stiffness matrix, K_e and global geometric stiffness matrix, K_G for the shell of revolution.

2.6 Displacement-dependent pressure

As it is mentioned before, Schweizerhof and Ramm (1984) divided loads into two groups, including: body attached and space attached. Space attached loads are the forces which both direction and magnitude of pressure change during acting force; while for body attached loads only directions are changed (Fig. 2).

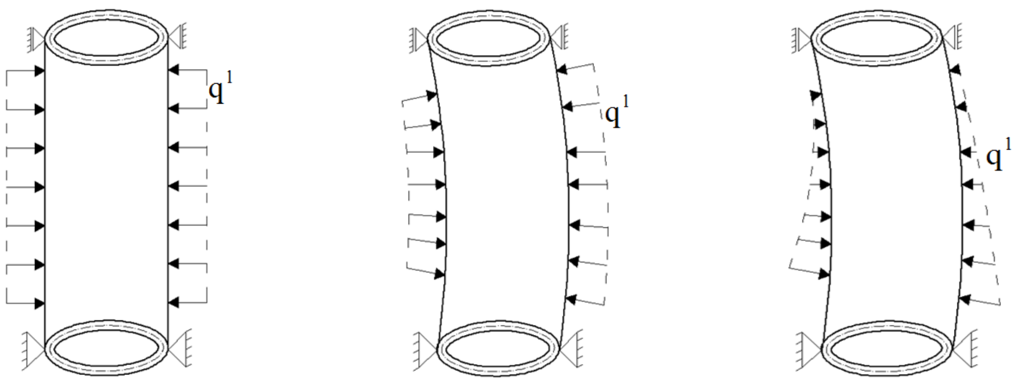

(a) Un-deformed

(b) Deformed
Body attached

(c) Deformed
Space attached load

Fig. 2 Loads definition

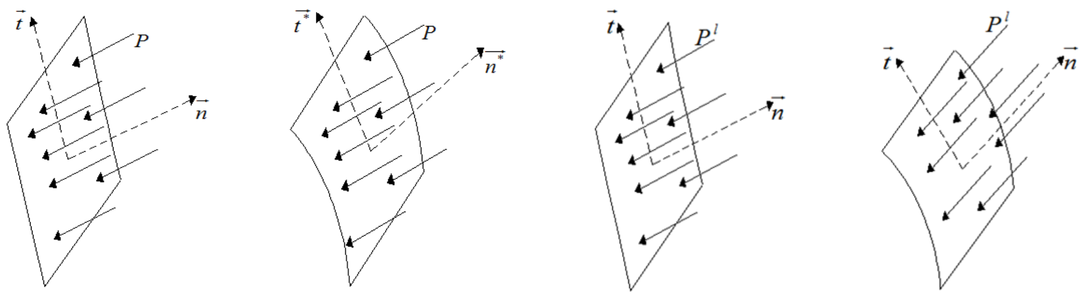

(a) Un-deformed (b) Deformed
Non-follower

(a) Un-deformed (b) Deformed
Follower

Fig. 3 Definition of follower and non-follower forces

The pressure stiffness matrix for the structures subjected to follower loads represents the effects of the change of loading direction and loaded area during their deformation, which can be formulated on the basis of the principle of virtual work. To calculate pressure stiffness for cylindrical shell, the following assumptions are adopted:

(1) Loading on the shell is perpendicular to the shell before and after deformation (Fig. 3)
(2) Loading acts on the shell middle surface.
(3) Shell deformations are small.
(4) Pressures are considered as body attached.

Position vector of an arbitrary point in the middle surface of shell of revolution is denoted $\vec{r}$ and $\vec{U}$ represents displacement vector of the point. Hence, the position vector in the deformed state is written as

$$\vec{r}^{\,*} = \vec{r} + \vec{U} \tag{17}$$

The components of $\vec{r}$ and $\vec{U}$ in terms of cylindrical coordinate system are as follows

$$\vec{r} = (R\cos\theta)\vec{i} + (R\sin\theta)\vec{j} + (Z)\vec{k} \tag{18}$$

$$\vec{U} = (w(s,\theta)\cos\theta - v(s,\theta)\sin\theta)\vec{i} + (w(s,\theta)\sin\theta + v(s,\theta)\cos\theta)\vec{j} + u(s,\theta)\vec{k} \tag{19}$$

The external virtual work, due to the follower forces, can be calculated based on the Eq. (20)

$$\delta W_{ext}^{P^l} = -\iint_S (P^l(s,\theta)dS^*\vec{n}^*)\cdot\delta\vec{U} \tag{20}$$

in which, p^1 can be non-uniform in both directions, s and θ, but it is assumed to be continuous function of them. dS^* is elemental area in the deformed state and $\vec{n}^*$ defines unit normal vector to the deformed shell middle surface. In addition, δU reflects infinitesimal virtual displacement vector of shell middle surface. According to vector analysis, the product of normal vector and differential element of deformed mid-surface area can be written as

$$dS^*\vec{n}^* = \begin{vmatrix} \vec{i} & \vec{j} & \vec{k} \\ \frac{\partial r_i^*}{\partial s} & \frac{\partial r_j^*}{\partial s} & \frac{\partial r_k^*}{\partial s} \\ \frac{\partial r_i^*}{\partial \theta} & \frac{\partial r_j^*}{\partial \theta} & \frac{\partial r_k^*}{\partial \theta} \end{vmatrix} ds d\theta \tag{21}$$

using Eqs. (21) and (20), the virtual work created by follower force is calculated as below

$$\begin{aligned}\delta W_{ext}^{P^l} = \iint P^l(s,\theta)\{&[\frac{\partial w}{\partial s} + \frac{v\frac{\partial v}{\partial s}}{R} + \frac{w\frac{\partial w}{\partial s}}{R} - \frac{\frac{\partial v}{\partial s}\frac{\partial w}{\partial \theta}}{R} + \frac{\frac{\partial v}{\partial \theta}\frac{\partial w}{\partial s}}{R}]\delta u + [-\frac{v}{R} + \frac{\frac{\partial w}{\partial \theta}}{R} + \frac{\frac{\partial w}{\partial \theta}\frac{\partial u}{\partial s}}{R} - \frac{\frac{\partial u}{\partial \theta}\frac{\partial w}{\partial s}}{R} - \frac{v\frac{\partial u}{\partial s}}{R}]\delta v \\ &+[-\frac{\partial Z}{\partial s} - \frac{\partial u}{\partial s} - \frac{\frac{\partial v}{\partial \theta}}{R} - \frac{w\frac{\partial u}{\partial s}}{R} - \frac{w}{R} - \frac{\frac{\partial u}{\partial s}\frac{\partial v}{\partial \theta}}{R} + \frac{\frac{\partial v}{\partial s}\frac{\partial u}{\partial \theta}}{R}]\delta w\} R ds d\theta\end{aligned} \tag{22}$$

In addition, potential operator is used to separate symmetric parts of total pressure stiffness matrix. It should be mentioned that the second order terms of displacements are removed because they have a little effect on the pressure stiffness matrix. Therefore, after integration by parts of Eq. (22), the virtual work of a cylindrical shell under follower forces is

$$\begin{aligned}\delta W_{ext}^{P^l} = &-\delta\iint P^l(s,\theta)(\frac{v^2}{2R} + \frac{w^2}{2R} + w\frac{\partial u}{\partial s} + w\frac{\partial v}{\partial \theta})ds d\theta + \int_0^{2\pi} P^l(s,\theta)\left(w\delta u R\right)_0^l \\ &+\iint \frac{\partial P^l(s,\theta)}{\partial s} R w \delta u ds d\theta + \iint \frac{\partial P^l(s,\theta)}{\partial \theta} w \delta v ds d\theta\end{aligned} \tag{23}$$

Fig. 4 presents a physical comprehension for different boundaries and loading conditions. Figs. 4(a) and (b) represent a non-conservative system because load is non-uniform and end of shell can move along horizontal direction. For the second structure; while Fig. 4(c) has support conditions

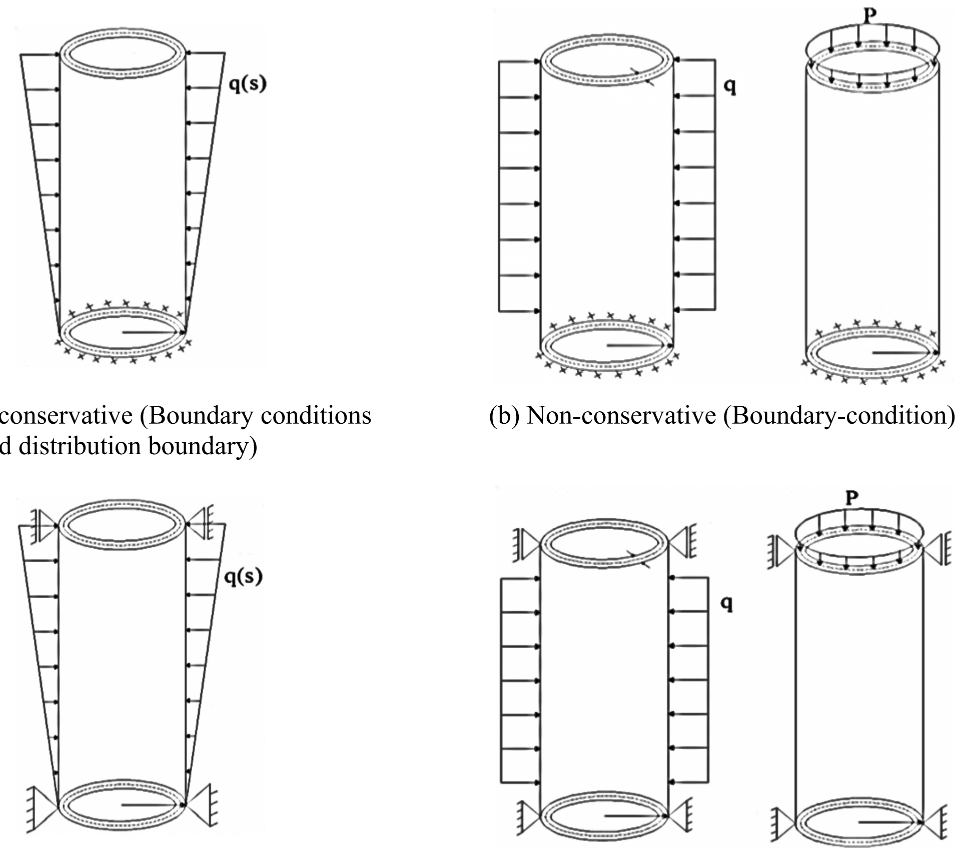

(a) Non-conservative (Boundary conditions + load distribution boundary)

(b) Non-conservative (Boundary-condition)

(c) non-conservative (Load distribution)

(d) Conservative

Fig. 4 Boundary and load conditions

leading to vanishing boundary terms according to Eq. (23), it should be noted that it is still a non-conservative system due to non-uniform distributed load. Fig. 4(d) also describes a conservative system since the free boundary is unloaded and the boundary integral in Eq. (23) vanishes.

If the pressure stiffness matrix is symmetric, it can be introduced as conservative system. Otherwise, if the pressure stiffness matrix is un-symmetric, it is called non-conservative system. In the case of conservative loads, static criterion (divergence) can be used which finally produces symmetric global stiffness matrix. In addition, non-conservative loads can cause system to be divided into purely or hybrid non-conservative system. The first group only fails by flutter and so the kinetic criterion, which connects computing buckling loads to vibration equation of structure, governs. In the hybrid case, both criteria, static or kinetic, can dominate the problem. In commercial programs such as Abaqus, pressure stiffness matrix is stored symmetrically (Goyal and Kapania (2008) - ABAQUS/standard user's manual (1998)). In all cases of this article, the static analysis (or divergence criterion) has been utilized in order to calculate the buckling load.

2.7 Eigenvalue problem

Having been formed global linear elastic stiffness matrix, K_e, global geometric stiffness K_G, and global load or pressure stiffness matrix K_P, the static criterion (divergence) for estimating load parameter λ_{cr} may be established through a linear eigenvalue analysis as follows

$$\left[K_e - \lambda_{cr}(K_G + K_P)\right]\Phi = 0 \tag{24}$$

λ_{cr} is the lowest eigenvalue and Φ is its associated eigenmode. As stated earlier, K_P is generally un-symmetric due to non-uniformity of loading and insufficient constraints in shell boundaries. In the sequel two types of eigenvalue analyses have been carried out, with pressure stiffness and without pressure stiffness. Comparison of the results of these two analyses to clarify the effect of considering or omitting K_P has been performed.

3. Numerical applications and results

Based on the above derivations, in this section, some results and considerations concerning the buckling loads problem of laminated composite cylindrical shells are presented. To verify the accuracy of the present method, some comparisons have been performed. Based on the presented formulations a computer program has been prepared to compute buckling pressure via eign-value problem.

3.1 The convergence study of finite strip method

The buckling of a simply supported cylindrical shell under lateral follower pressure for different number of strips is considered. The lay-up of shell is ($[0/0/90]_s$), radius, thickness and length of the cylinder are 190.5, 6.35 and 762 mm, respectively. The material properties are considered as

$$E_{11} = 130 \text{ GPa} \quad E_{22} = 7 \text{ GPa} \quad G_{12} = G_{13} = 6 \text{ GPa}$$
$$G_{23} = 4.2 \text{ GPa} \quad \upsilon_{12} = 0.28$$

Variations of follower buckling pressure of the cylinder with regard to different number of strips in the meridian direction is depicted in Fig. 5.

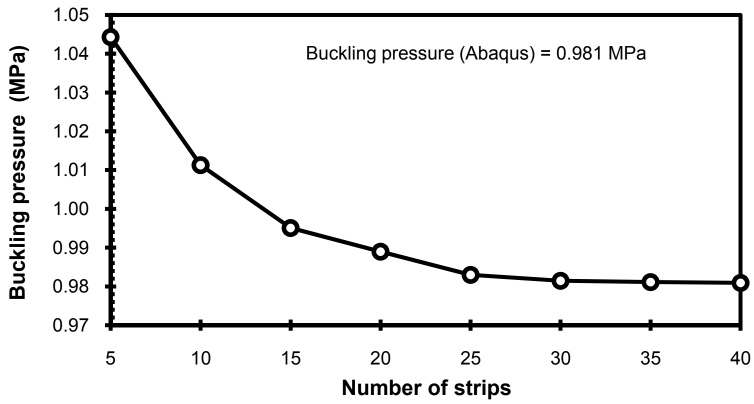

Fig. 4 Boundary and load conditions

For all models considered in the example, minimum buckling pressure is obtained with circumferential wave number, n_{cr} = 4. As it is seen from Fig. 4 the buckling pressure nearly remains unchanged after considering 30 strips in the model but to cover variations in geometry, shell lay-up and boundary conditions, in the following problems 40 strips have been taken in the meridian direction. It is to be noted that the FEM result obtained by Abaqus software using (3724) S8R5 elements is also shown in the Fig. 5.

3.2 Laminated (cross ply) cylinder under lateral pressure

In this section, the buckling analyses are carried out for cylindrical shells having two fixed ends under uniform lateral pressure. Therefore, the effects of different properties such as, shell thickness, length to radius ratio and lay-ups ($[90/90/90]_s$, $[0/90/0]_s$) by considering the presence and absence of pressure stiffness (follower action) on critical lateral pressure have been compared to those of other research results. Radius of the cylinder is 190.5 mm. The material properties are considered as

$$E_{11} = 206.844 \text{ GPa} \quad E_{22} = 18.6159 \text{ GPa} \quad G_{12} = G_{13} = 4.482 \text{ GPa}$$

$$G_{23} = 2.55107 \text{ GPa} \quad \upsilon_{12} = \upsilon_{13} = 0.21 \quad \upsilon_{23} = 0.25$$

In this study, the difference between the calculated buckling load by considering and neglecting the pressure stiffness is shown by the Eq. (25)

$$\mu(\%) = \left(\frac{q_{cr(\text{without PS})} - q_{cr(\text{with PS})}}{q_{cr(\text{with PS})}} \right) 100 \tag{25}$$

The results are presented in Tables 1-2.

According to Tables 1-2, the calculated buckling results are in accordance with the investigated results done in Cagdas and Adali (2011) by considering two different states, with and without pressure stiffness. One reason for difference between these two studies is that Cagdas and Adali

Table 1 Buckling pressure (MPa) of cylindrical shell under lateral pressure for lay-up $[90/90/90]_s$

h (mm)	L/R	N	Cagdas and Adali (2011) without PS	Cagdas and Adali (2011) with PS	Cagdas and Adali (2011) μ (%)	Current study without PS	Current study with PS	μ (%)
3.175	1	5	3.417	3.301	3.5	3.402	3.283	3.6
	2	4	1.946	1.838	5.9	1.940	1.830	6.0
	5	3	0.941	0.843	11.6	0.940	0.841	11.7
6.35	1	5	18.521	17.957	3.1	18.432	17.480	5.4
	2	3	11.087	10.037	10.5	10.969	9.892	10.9
	5	3	5.990	5.388	11.2	5.979	5.353	11.7
12.7	1	4	92.293	88.672	4.1	91.311	86.464	5.6
	2	3	52.581	48.225	9.0	51.981	46.897	10.8
	5	2	28.275	22.220	27.3	27.890	21.554	29.4

Table 2 Buckling pressure (MPa) of cylindrical shell under lateral pressure for lay-up $[90/90/90]_s$

h (mm)	L/R	N	Cagdas and Adali (2011) without PS	Cagdas and Adali (2011) with PS	Cagdas and Adali (2011) μ (%)	Current study without PS	Current study with PS	μ (%)
3.175	1	7	2.283	2.240	1.9	2.283	2.239	2.0
	2	5	1.085	1.044	4.0	1.085	1.043	4.0
	5	4	0.532	0.499	6.5	0.532	0.499	6.6
6.35	1	6	14.878	14.517	2.5	14.875	14.481	2.7
	2	4	6.175	5.820	6.1	6.163	5.796	6.3
	5	3	2.794	2.495	12.0	2.790	2.487	12.2
12.7	1	5	88.224	86.351	2.2	88.248	85.670	3.0
	2	4	34.719	32.921	5.5	34.656	32.584	6.4
	5	3	16.294	14.652	11.2	16.268	14.497	12.2

(2011) has applied the Koiter – Sanders relations to calculate the pressure stiffness.

In another parametrics buckling analysis, the results for six L/R (1, 2, 4, 8, 10, 20), there thicknesses (3.175, 6.35, 12.7 mm) and eight stacking sequences for the pined-pined cylindrical shell under uniform lateral pressure, have been presented in Table 3.

The maximum lateral buckling pressure occurs in lay-up $[90/90/0]_s$ for two types of analysis, with and without pressure stiffness. According to Table 3 for cylindrical shell under uniform lateral pressure, increasing in thickness and length to reduce ratio intensify the effect of follower action on the buckling pressure.

3.3 Laminated cylinder under lateral pressure (*Symmetric and un- symmetric lay-ups*)

In this section, the effects of pressure stiffness and bending-extensional rigidity, B_{ij}, on buckling pressure are investigated for pined-pined cylindrical shells. The shell comprises of a four-ply laminate with balanced symmetric stacking sequence $[\theta/0/-\theta]_s$ and un-symmetric stacking sequence $[\theta/0/-\theta]_2$ in which θ varies from 0 to 90 degrees. For symmetric lay-up $[\theta/0/-\theta]_s$, the bending-extension coupling, $B_{ij} = 0$, but for un-symmetric lay-up $[\theta/0/-\theta]_2$, $B_{ij} \neq 0$. Various length to radius ratios and different shell thicknesses are considered in the analyses. The calculated non-follower and follower buckling loads are shown in Tables 4-9 for different L/R, h (thickness) and fiber orientation, θ. Forty, two-nodded strips have been taken into account in the meridian direction. It should be mentioned that the results were generated for the following geometry and material properties (Graphite/epoxy)

$$E_1 = 130\,\text{GPa} \quad E_2 = 7\,\text{GPa} \quad G_{12} = G_{13} = 6\,\text{GPa} \quad G_{23} = 4.2\,\text{GPa} \quad \upsilon_{12} = \upsilon_{13} = 0.28$$
$$R = 300\,\text{mm}$$

According to Tables 4-9, it has been concluded that the maximum effect of follower force on the buckling load is nearly 32%. In other words, if the pressure stiffness matrix is neglected, shell is designed for a pressure nearly one third larger than the pressure which causes buckling. According to Tables 4-9, for a thin shell, if the length to radius ratio in every stacking sequences as

Table 3 Buckling pressure (MPa) of cylindrical shell under uniform lateral pressure for cross-ply laminates

	L/R	1			2			4			8			10			20		
	Lay-up	$*P_1$	$**P_2$	$***\mu$	P_1	P_2	μ	P_1	P_2	μ	P_1	P_2	μ	P_1	P_2	μ	P_1	P_2	μ
$H = 3.175$	[0]3s	0.489	0.485	0.81	0.247	0.242	1.85	0.137	0.133	2.75	0.080	0.076	6.17	0.062	0.059	6.58	0.034	0.030	12.42
	[90]3s	2.372	2.322	2.18	1.347	1.279	5.32	0.735	0.663	10.79	0.474	0.400	18.45	0.340	0.261	30.64	0.210	0.159	32.58
	[0/0/90]s	0.645	0.638	1.16	0.335	0.329	2.01	0.190	0.182	4.07	0.103	0.096	6.57	0.087	0.082	6.59	0.047	0.042	12.42
	[0/90/90]s	1.349	1.324	1.91	0.781	0.761	2.72	0.445	0.418	6.41	0.253	0.226	12.15	0.201	0.179	12.23	0.123	0.093	32.72
	[0/90/0]s	1.270	1.247	1.88	0.736	0.716	2.74	0.452	0.425	6.35	0.271	0.245	10.89	0.207	0.185	12.28	0.142	0.112	26.99
	[90/90/0]s	2.528	2.464	2.61	1.561	1.502	3.93	0.944	0.887	6.41	0.536	0.478	12.15	0.484	0.431	12.23	0.250	0.188	32.72
	[90/0/90]s	2.187	2.132	2.59	1.308	1.258	3.93	0.779	0.732	6.41	0.442	0.394	12.14	0.390	0.347	12.23	0.208	0.156	32.72
	[90/0/0]s	2.123	2.071	2.54	1.292	1.243	3.95	0.785	0.738	6.46	0.463	0.413	12.22	0.396	0.353	12.28	0.233	0.175	32.80
$H = 6.35$	[0]3s	3.377	3.335	1.27	1.336	1.304	2.42	0.747	0.719	3.95	0.431	0.405	6.53	0.374	0.333	12.18	0.215	0.192	12.43
	[90]3s	12.601	12.231	3.03	7.431	7.053	5.36	4.139	3.735	10.81	2.221	1.716	29.47	1.868	1.430	30.66	1.613	1.217	32.58
	[0/0/90]s	3.978	3.909	1.76	1.871	1.821	2.72	1.044	0.981	6.46	0.612	0.546	12.22	0.473	0.422	12.28	0.322	0.243	32.80
	[0/90/90]s	7.530	7.343	2.55	4.232	4.050	4.50	2.522	2.370	6.41	1.417	1.264	12.15	1.308	1.165	12.23	0.650	0.490	32.72
	[0/90/0]s	7.067	6.895	2.50	3.933	3.785	3.93	2.367	2.223	6.46	1.365	1.216	12.23	1.226	1.092	12.29	0.659	0.496	32.80
	[90/90/0]s	12.958	12.495	3.71	8.020	7.551	6.21	4.877	4.361	11.83	3.628	2.765	31.19	2.644	2.006	31.82	1.649	1.243	32.72
	[0/90/0]s	11.357	10.956	3.66	6.797	6.401	6.20	4.155	3.716	11.83	2.898	2.516	15.20	2.315	1.756	31.81	1.318	0.993	32.73
	[90/0/0]s	10.919	10.548	3.52	6.645	6.258	6.18	4.206	3.758	11.92	2.844	2.534	12.24	2.583	1.955	32.13	1.326	0.998	32.82
$H = 12.7$	[0]3s	30.848	30.194	2.17	7.829	7.575	3.36	4.022	3.792	6.08	2.289	2.044	12.02	1.961	1.748	12.21	1.158	0.873	32.70
	[90]3s	63.193	60.474	4.50	37.213	34.101	9.13	24.980	20.135	24.06	13.593	10.495	29.52	12.904	9.873	30.70	12.399	9.372	32.30
	[0/0/90]s	26.780	26.265	1.96	10.632	10.234	3.89	5.808	5.456	6.45	3.226	2.874	12.23	2.915	2.596	12.29	1.514	1.140	32.81
	[0/90/90]s	44.500	42.924	3.67	22.246	20.956	6.16	12.730	11.382	11.84	8.552	6.505	31.47	6.525	4.949	31.84	4.482	3.376	32.74
	[0/90/0]s	43.158	41.643	3.64	20.632	19.444	6.11	12.086	10.799	11.92	8.990	6.820	31.82	6.729	5.092	32.15	4.167	3.137	32.84
	[90/90/0]s	64.008	60.598	5.63	40.586	36.481	11.25	28.719	25.670	11.88	16.136	12.271	31.50	14.145	10.726	31.88	12.157	9.154	32.80
	[0/90/0]s	60.082	56.908	5.58	35.939	32.320	11.20	23.587	21.086	11.86	13.653	10.383	31.49	11.649	8.835	31.86	9.642	7.262	32.77
	[90/0/0]s	58.293	55.375	5.27	34.921	31.471	10.96	22.877	20.431	11.97	14.086	10.681	31.88	11.847	8.961	32.20	9.316	7.010	32.89

* P_1 is buckling pressure without pressure stiffness; ** P_2 is buckling pressure with pressure stiffness

*** $\mu = \dfrac{P_1 - P_2}{P_2} \times 100$

Table 4 Buckling pressure (MPa) of cylindrical shell under lateral pressure for symmetric lay-up, h = 3 mm

L/R		2			5			10	
θ	Non-follower	Follower	μ (%)	Non-follower	Follower	μ (%)	Non-follower	Follower	μ (%)
10	0.085	0.084	1.15	0.036	0.035	2.79	0.019	0.018	4.13
20	0.106	0.105	1.06	0.044	0.043	2.79	0.023	0.022	4.14
30	0.142	0.140	1.15	0.058	0.056	2.80	0.030	0.028	6.59
40	0.195	0.193	1.15	0.083	0.081	2.79	0.042	0.039	6.59
50	0.264	0.260	1.45	0.112	0.108	4.03	0.061	0.057	6.57
60	0.337	0.331	1.89	0.148	0.142	4.02	0.085	0.076	12.17
70	0.392	0.385	1.92	0.183	0.172	6.36	0.095	0.085	12.17
80	0.401	0.390	2.67	0.187	0.176	6.41	0.102	0.091	12.21
90	0.395	0.385	2.71	0.186	0.175	6.45	0.103	0.092	12.23

Table 5 Buckling pressure (MPa) of cylindrical shell under lateral pressure for symmetric lay-up, h = 15 mm

L/R		2			5			10	
θ	Non-follower	Follower	μ (%)	Non-follower	Follower	μ (%)	Non-follower	Follower	μ (%)
10	5.557	5.426	2.42	1.934	1.821	6.22	1.037	0.925	12.15
20	6.442	6.304	2.19	2.407	2.267	6.17	1.257	1.121	12.15
30	8.031	7.862	2.15	3.198	3.011	6.21	1.683	1.501	12.17
40	10.496	10.269	2.21	4.463	4.203	6.19	2.452	2.187	12.10
50	13.790	13.361	3.21	6.319	5.956	6.08	3.629	3.241	11.96
60	16.824	16.285	3.31	7.886	7.083	11.34	5.169	3.983	29.79
70	19.507	18.487	5.52	9.084	8.148	11.49	5.622	4.287	31.14
80	19.734	18.632	5.91	9.926	8.883	11.74	5.760	4.378	31.54
90	19.865	18.720	6.12	10.239	9.149	11.92	5.718	4.338	31.80

Table 6 Buckling pressure (MPa) of cylindrical shell under lateral pressure for symmetric lay-up, h = 30 mm

L/R		2			5			10	
θ	Non-follower	Follower	μ (%)	Non-follower	Follower	μ (%)	Non-follower	Follower	μ (%)
10	41.734	40.142	3.97	11.576	10.443	10.85	6.405	5.709	12.19
20	43.503	42.126	3.27	14.390	13.193	9.07	7.709	6.876	12.12
30	48.374	46.977	2.97	18.851	17.021	10.75	10.478	9.355	12.01
40	58.281	56.575	3.02	24.624	22.190	10.97	15.372	11.829	29.95
50	73.092	70.899	3.09	32.399	29.198	10.96	19.297	14.767	30.68
60	87.44	83.322	4.94	42.014	37.874	10.93	24.206	18.512	30.76
70	100.09	94.985	5.37	52.505	47.266	11.08	29.123	22.228	31.02
80	105.86	95.766	10.54	57.684	44.531	29.54	32.732	24.889	31.51
90	102.49	92.296	11.04	53.789	41.270	30.33	34.066	25.835	31.86

Table 7 Buckling pressure (MPa) of cylindrical shell under lateral pressure for un-symmetric lay-up, h = 3 mm

L/R	2			5			10		
θ	Non-follower	Follower	μ (%)	Non-follower	Follower	μ (%)	Non-follower	Follower	μ (%)
10	0.084	0.083	1.15	0.036	0.035	2.79	0.019	0.018	4.13
20	0.106	0.105	1.15	0.043	0.041	2.79	0.022	0.021	4.14
30	0.140	0.139	1.18	0.054	0.053	2.81	0.028	0.026	6.60
40	0.191	0.188	1.48	0.077	0.074	3.60	0.037	0.035	6.60
50	0.250	0.246	1.50	0.099	0.095	4.05	0.052	0.049	6.59
60	0.308	0.302	1.93	0.129	0.124	4.04	0.073	0.068	6.87
70	0.359	0.352	1.96	0.163	0.156	4.05	0.086	0.077	12.18
80	0.383	0.373	2.69	0.178	0.167	6.42	0.097	0.086	12.21
90	0.395	0.385	2.71	0.186	0.175	6.45	0.103	0.092	12.23

Table 8 Buckling pressure (MPa) of cylindrical shell under lateral pressure for un-symmetric lay-up, h = 15 mm

L/R	2			5			10		
θ	Non-follower	Follower	μ (%)	Non-follower	Follower	μ (%)	Non-follower	Follower	μ (%)
10	5.618	5.483	2.46	1.929	1.816	6.23	1.031	0.919	12.15
20	6.763	6.609	2.34	2.387	2.247	6.23	1.226	1.093	12.17
30	8.782	8.576	2.40	3.163	2.975	6.33	1.601	1.426	12.24
40	11.588	11.212	3.35	4.454	4.186	6.41	2.308	2.056	12.27
50	14.333	13.840	3.56	6.124	5.496	11.42	3.402	3.031	12.26
60	17.318	16.696	3.73	7.169	6.427	11.53	4.769	3.642	30.94
70	18.764	17.736	5.80	8.289	7.421	11.70	5.142	3.919	31.21
80	19.305	18.200	6.07	9.460	8.455	11.88	5.486	4.169	31.59
90	19.865	18.720	6.12	10.239	9.149	11.92	5.718	4.338	31.80

well as thickness of the shells increases, the effect of pressure stiffness on the buckling load increases as well. For instance, as you can see in Table 5, for the thickness equals to 15 mm and L/R = 2, the maximum effect of follower action on the buckling force is 6.12% (μ_{max} = 6.12) while for ratio L/R = 10, μ_{max} = 31.8. In addition, increasing thickness acquires the similar result with unchanging length to radius ratio so that for L/R = 2 and t = 3 mm (Table. 7), the lowest effect of this assumption on the buckling pressure is 1.15% (μ_{max} = 1.15), while for thickness equals to 30 mm and L/R = 2, μ_{max} = 4.02%. Furthermore, for the latter thickness and L/R, the maximum effects of this assumption on the buckling are 2.71% and 11.04%, respectively. Therefore, the effect of increasing length to radius ratio is more than that of increasing thickness on the value of μ. Another issue that can be perceived from Tables 4-9 is that different influences of pressure stiffness matrix on buckling pressure are variable with fiber orientation, as by increasing angle of fiber from 10 to 90 degrees, the effects of follower loading on the buckling pressure increases. The

Table 9 Buckling pressure (MPa) of cylindrical shell under lateral pressure for un-symmetric lay-up, h = 30 mm

L/R	2			5			10		
θ	Non-follower	Follower	μ (%)	Non-follower	Follower	μ (%)	Non-follower	Follower	μ (%)
10	42.102	40.473	4.02	11.556	10.419	10.91	6.405	5.707	12.21
20	46.002	44.430	3.54	14.537	13.130	10.72	7.750	6.905	12.24
30	54.201	52.399	3.44	18.720	16.858	11.05	10.822	9.556	13.25
40	67.505	65.177	3.57	24.430	21.929	11.40	14.383	11.002	30.73
50	80.634	76.645	5.20	32.168	28.823	11.61	17.527	13.385	30.95
60	92.245	87.345	5.61	41.398	37.040	11.77	21.695	16.544	31.14
70	102.820	97.015	5.98	51.170	45.699	11.97	26.304	20.014	31.43
80	104.520	94.359	10.77	55.839	43.051	29.70	31.068	23.578	31.77
90	102.490	92.296	11.04	53.789	41.270	30.33	34.066	25.835	31.86

maximum buckling pressure for the two lay-ups and with and without pressure stiffness, induces in two stacking sequences including θ = 80 and 90 degrees. In addition, the effects of bending-extension rigidity, B_{ij}, on follower buckling pressure are not sizeable so that a comparison between the calculated values of μ for two lay-ups $[\theta/0/-\theta]_s$ and $[\theta/0/-\theta]_2$ reveals that they are approximately equal.

3.4 Laminated cylinder under combined Lateral and axial pressures

In this section, the effects of pressure stiffness on buckling load for the fixed-fixed cylinders under hydrostatic pressure (combined lateral and axial pressures) for various lay-ups, length to radius ratios and different thicknesses are investigated. The shell comprises of a four-ply laminate with balanced symmetric stacking sequences $[\alpha/-\alpha]_s$ in which α varies from 0 to 90 degrees. The results are shown in Figs. 6-8 for two states, non-follower and follower buckling. The considered material properties and shell radius are

$$E_1 = 206.844 \text{ GPa} \quad E_2 = 18.6159 \text{ GPa} \quad G_{12} = G_{13} = 4.482 \text{ GPa} \quad G_{23} = 2.55107 \text{ GPa}$$
$$\upsilon_{12} = \upsilon_{13} = 0.21 \quad \upsilon_{23} = 0.25 \qquad R = 190.5\,\text{mm}$$

Hydrostatic pressure has the same effects as lateral pressure when the forces are assumed as follower type. It should be noted that hydrostatic pressure effect, due to presence of pressure stiffness, is slightly more in comparison with the other kind of pressure. Another point which can be determined by considering Figs. 6-8 is that the differences in influence of pressure stiffness matrix on buckling pressure depend on angle of fibers, as with increasing angle of fiber from 5 to 90 degrees, the effects of follower-type loading on the buckling pressure increases.

By using cylindrical shells analyses with different geometries and lay-ups, it is determined that a relation exists between buckling mode (number of circumferential wave, n_{cr}) and follower effects on buckling load so that by reducing the number of waves, the effect of follower force on buckling pressure increases and its maximum value occurs for n_{cr} = 2, as you can observe in Table 10.

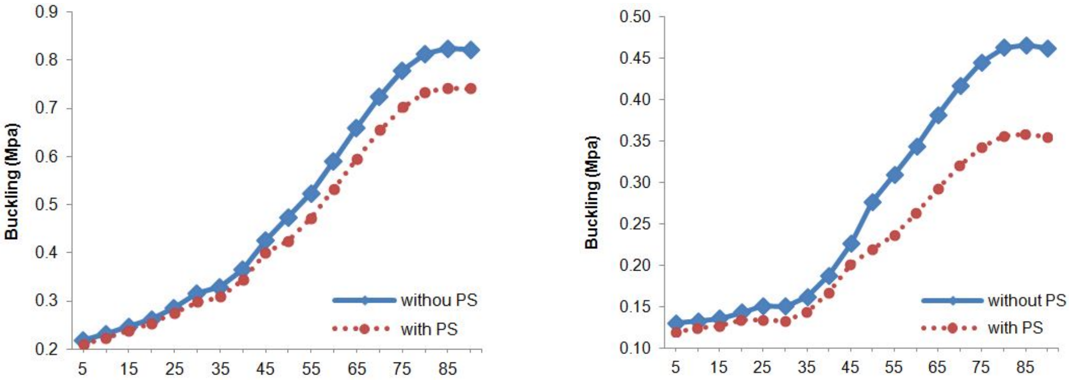

(a) (b)

Fig. 6 Buckling load for fixed-fixed cylindrical shell for two loading types, follower and non-follower, for h = 3.175 mm and L/R = 5 and 10

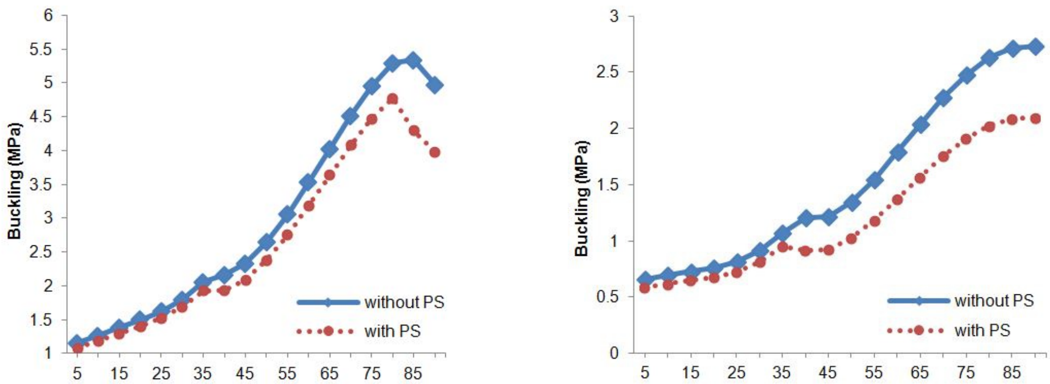

(a) (b)

Fig. 7 Buckling load for fixed-fixed cylindrical shell for two loading types, follower and non-follower for h = 6.35 mm and L/R = 5 and 10

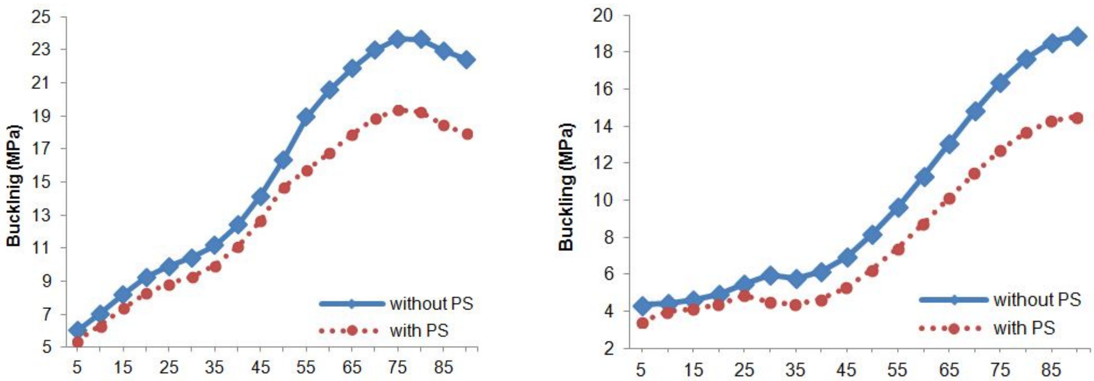

(a) (b)

Fig. 8 Buckling load for fixed-fixed cylindrical shell for two loading types, follower and non-follower for h = 12.7 mm and L/R = 5 and10

Table 10 Buckling pressure for (h = 3.175 mm, L/R = 10)

Lay-up	Non-follower	Follower	Number of wave (n_{cr})	μ (%)
[5/-5]s	0.130	0.119	4	8.64
[10/-10]s	0.132	0.124	4	6.59
[15/-15]s	0.135	0.127	4	6.62
[20/-20]s	0.143	0.134	4	6.65
[25/-25]s	0.151	0.134	3	12.48
[30/-30]s	0.150	0.133	3	12.51
[35/-35]s	0.162	0.144	3	12.47
[40/-40]s	0.187	0.167	3	12.39
[45/-45]s	0.226	0.201	3	12.27
[50/-50]s	0.276	0.220	2	25.60
[55/-55]s	0.309	0.237	2	30.59
[60/-60]s	0.344	0.264	2	30.28
[65/-65]s	0.381	0.293	2	30.06
[70/-70]s	0.417	0.321	2	29.91
[75/-75]s	0.445	0.343	2	29.84
[80/-80]s	0.463	0.356	2	29.88
[85/-85]s	0.466	0.358	2	30.04
[90/-90]s	0.462	0.355	2	30.17

Inspection of buckling modes for different shell geometries and lay-ups reveals that in addition to changing in circumferential wave number, n_{cr}, amplitudes of the modes components, v, w, u, β_s and β_θ are also altered relatively. These changes affect both on the direction of normal vector to the shell middle surface and the deformed area in the buckling process. Thus, these two factors cause different effects due to considering follower-type pressure in the analyses.

By considering the results of this study, the maximum value of μ for every number of circumferential waves (n_{cr}) is shown in Fig. 9.

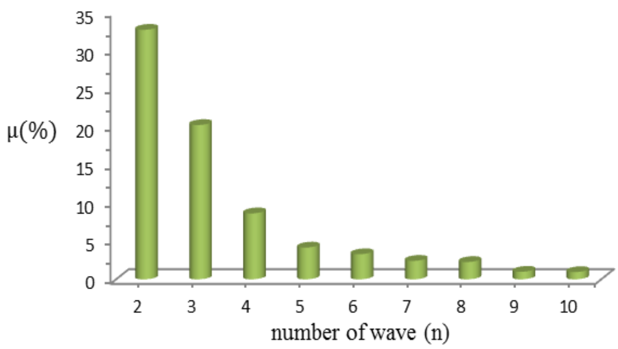

Fig. 9 Maximum effect of pressure stiffness on buckling pressure μ (%) for different circumferential wave numbers (n_{cr})

According to Fig. 9, it can be concluded that taking into account the pressure stiffness in buckling analysis under follower pressures for circumferential wave less than n_{cr} = 8 is required, while for more than n_{cr} = 8, it can be removed.

4. Conclusions

In this paper, the buckling behavior of the laminated cylindrical shells was investigated under follower pressure. Firstly, the shell is divided into several closed strips with alignment of their nodal lines in the circumferential direction. Afterwards, displacements and rotations in the shell middle surface are approximated by combining polynomial functions in the meridional direction and truncated Fourier series having an appropriate number of harmonic terms in the circumferential direction. In the next step, linear elastic stiffness, geometric stiffness and pressure stiffness are calculated for each strip and finally these matrices are assembled for the whole shell.

Therefore, based on the presented results, the reader comprehends the importance of displacement dependent pressure in designing thin-walled cylindrical shells. The numerical results support the following conclusions:

- Results reveal that the effect of follower action on buckling pressure increases for cylindrical shell when length to radius ratio and thickness goes up. Moreover, the effect of length to radius ratio variations is higher than the influence of thickness changes.
- The effect of bending-extension rigidity (B_{ij}) is not sizeable on buckling pressure when pressure is assumed as follower type.
- The effect of pressure stiffness on buckling for hydrostatic pressure is similar to that of lateral pressure.
- The results show that increasing the effect of considering pressure stiffness on buckling pressure is along with decreasing circumferential wave number.

References

ABAQUS/standard user's manual (1998), Vols. I–III, Version 5.8: Hibbitt, Karlsson & Sorensen, Inc., Pawtucket, RI, USA.

Altman, W. and Oliveira, M.G.D. (1988), "Vibration and Stability cantilevered cylindrical shell panels under follower forces", *J. Sound Vib*., **122**(2), 291-298.

Altman, W. and Oliveira, M.G.D. (1990), "Vibration and Stability shell panels with slight internal damping under follower forces", *J. Sound Vib*., **136**(1), 45-50.

Altman, W. and Oliveira, M.G.D. (1987), "Stability of cylindrical shell panels subjected to follower forces based on a mixed finite element formulation", *Comput. Struct*., **27**(3), 367-372.

Anastasiadis, J.S. and Simitses, G.J. (1993), "Buckling of pressure-loaded, long, shear deformable, cylindrical laminated shells", *J. Compos. Struct*., **23**(3), 221-231.

Argyris, J.H. and Symeonidis, Sp. (1981), "Nonlinear finite element analysis of elastic system under nonconservative loading – natural formulation, part1, quasistatic problems", *Comput. Method. Appl. Mech. Eng*., **26**(1), 75-123.

Bolotin, V.V. (1963), *Nonconservative Problems of the Theory of Elastic Stability*, Pergamon Press, New York, NY, USA, pp. 53-55.

Cagdas, I.U. and Adali, S. (2011), "Buckling of cross-ply cylinders under hydrostatic pressure considering pressure stiffness", *Ocean Eng*., **38**(4), 559-569.

Cohen, G.A. (1966), "Conservative of a normal pressure field acting on a shell", *AIAA*, **4**(10).

Datta, P.K. and Biswas, S. (2011), "Aeroelastic behaviour of aerospace structural Elements with Follower Force: A review", *J. Aeronaut. Space Sci.*, **12**(2), 134-148.

Goyal, V.K. and Kapania, R.K. (2008), "Dynamic stability of laminated beams subjected to nonconservative loading", *Thin-Wall. Struct.*, **46**(12), 1359-1369.

Hibbitt, H.D. (1979), "Some follower forces and load stiffness", *Int. J. Numer. Method. Eng.*, **14**(6), 207-231.

Iwata, K., Tsukimor, K. and Kubo, F. (1991), "A symmetric load-stiffness matrix for buckling analysis of shell structures under pressure loads", *Int. J. Press. Ves. Piping*, **45**(1), 101-120.

Jung, W.Y., Han, S.C., Lee, W.H. and Park, W.T. (2016), "Postbuckling analysis of laminated composite shells under shear loads", *Steel Compos. Struct.*, *Int. J.*, **21**(2), 373-394.

Khayat, M., Poorveis, D., Moradi, S. and Hemmati, M. (2016), "Buckling of thick deep laminated composite shell of revolution under follower forces", *Struct. Eng. Mech.*, *Int. J.*, **58**(1), 59-91.

Lazzari, M., Vitaliani, R.V., Majowiecki, M. and Saett, A.V. (2003), "Dynamic behavior of a tensegrity system subjected to follower wind loading", *Comput. Struct.*, **81**(22-23), 2199-2217.

Li, Z.M. and Lin, Z.Q. (2010), "Non-linear buckling and postbuckling of shear deformable anisotropic laminated cylindrical shell subjected to varying external pressure loads", *Compos. Struct.*, **92**(2), 553-567.

Matsunaga, H. (2007), "Vibration and buckling of cross-ply laminated composite circular cylindrical shells according to a global higher-order theory", *Int. J. Mech. Sci.*, **49**(9), 1060-1075.

Nali, P., Carrera, E. and Lecca, S. (2011), "Assessments of refined theories for buckling analysis of laminated plates", *Compos. Struct.*, **93**(2), 456-464.

Ovesy, H.R. and Fazilati, J. (2009), "Stability analysis of composite laminated plate and cylindrical shell structures using semi-analytical finite strip method", *Compos. Struct.*, **89**(3), 467-474.

Park, S.H. and Kim, J.H. (2002), "Dynamic stability of a stiff-edged cylindrical shell subjected to a follower force", *Comput. Struct.*, **80**(3-4), 227-233.

Poorveis, D. and Kabir, M.Z. (2006), "Buckling of discretely stringer-stiffened composite cylindrical shells under combined axial compression and external pressure", *Scientia Iranica*, **13**(2), 113-123.

Romano, G. (1971), "Potential operators and conservative systems", *Proceedings of the 14th Polish Solid Mechanics Conference*, Kroscjenko, Poland, September.

Schweizerhof, K. and Ramm, E. (1984), "Displacement dependent pressure loads in nonlinear finite element analysis", *Comput. Struct.*, **18**(6), 1099-1114.

Sheinman, I. and Tene, Y. (1974), "Potential energy of a normal pressure field acting on an arbitrary shell", *AIAA*, **11**(8), 1216a-1216.

Shen, H.S. (1998), "Postbuckling analysis of stiffened laminated cylindrical shells under combined external liquid pressure and axial compression", *Eng. Struct.*, **20**(8), 738-751.

Simitses, G.J., Tabiei, A. and Anastasiadis, J.S. (1993), "Buckling of moderately thick, laminated cylindrical shells under lateral pressure", *J. Compos. Eng.*, **3**(5), 409-417.

Teng, J.G. and Hong, T. (1998), "Nonlinear thin shell theories for numerical buckling predictions", *Thin-Wall. Struct.*, **31**(1-3), 89-115.

Tornabene, F., Fantuzzi, N. and Bacciocchi, M. (2014), "Free vibrations of free-form doubly-curved shells made of functionally graded materials using higher-order equivalent single layer theories", *Compos. Part B: Eng.*, **67**, 490-509.

Tornabene, F., Fantuzzi, N., Bacciocchi, M. and Viola, E. (2015), "A new approach for treating concentrated loads in doubly-curved composite deep shells with variable radii of curvature", *Compos. Struct.*, **131**, 433-452.

Wang, Q. (2003), "On complex flutter and buckling analysis of a beam structure subjected to static follower force", *Struct. Eng. Mech.*, *Int. J.*, **16**(5), 533-556.

Zielnica, J. (2012), "Buckling and stability of elastic-plastic sandwich conical shells", *Steel Compos. Struct.*, *Int. J.*, **13**(2), 157-169.

CC